Nonlinear interdecadal changes of the El Niño-Southern Oscillation

Aiming Wu and **William W. Hsieh**

Dept. of Earth and Ocean Sciences, University of British Columbia

Vancouver, B.C., Canada, V6T 1Z4

Tel: (604) 822-3932, Fax: (604) 822-6088

Email: awu@eos.ubc.ca

June 23, 2003

Abstract

Nonlinear interdecadal changes in the El Niño-Southern Oscillation (ENSO) phenomenon are investigated using several tools— a nonlinear canonical correlation analysis (NLCCA) method based on neural networks, a hybrid coupled model, and the delayed oscillator theory. The leading NLCCA mode between the tropical Pacific wind stress (WS) and sea surface temperature (SST) reveals notable interdecadal changes of ENSO behaviour before and after the mid 1970s climate regime shift, with greater nonlinearity found during 1981-99 than during 1961-75. Spatial asymmetry (for both SST and WS anomalies) between warm El Niño and cool La Niña events was significantly enhanced in the later period. During 1981-99, the location of the equatorial easterly anomalies was unchanged from the earlier period, but in the opposite ENSO phase, the westerly anomalies were shifted eastward by up to 25°. According to the delayed oscillator theory, such an eastward shift would lengthen the duration of the warm events by up to 45%, but leave the duration of the cool events unchanged. Supporting evidence was found from a hybrid coupled model built with the Lamont dynamical ocean model coupled to a statistical atmospheric model consisting of either the leading NLCCA or CCA mode.

1 Introduction

The mid 1970s climate regime shift is an abrupt change in the SST and large-scale atmospheric circulation observed over the North Pacific (Trenberth 1990; Trenberth and Hurrell 1994). An analysis of the 40-year (1951-1990) Comprehensive Ocean-Atmosphere Data Set (COADS) revealed that the onset and development characteristics of El Niño had experienced a significant change after the 1976-77 El Niño (Wang 1995). The dominant period of the El Niño increased from 2-3 years during the 1960s and 1970s to 4-5 years during the 1980s and 1990s (Gu and Philander 1995; Wang and Wang 1996); during this time the amplitude of El Niño also increased (An and Wang 2000). These changes were accompanied by a notable modification in the evolution pattern and spatial structure of the coupled ocean-atmospheric anomalies. During the 1960s and 1970s, the warm SST anomalies expanded westward from the South American coast into the central equatorial Pacific (Rasmusson and Carpenter 1982); after 1980, the warm SST anomalies propagated eastward across the basin from the central Pacific or developed concurrently in the central and eastern Pacific (Wallace et al. 1998). Moreover, ENSO prediction skills of the coupled ocean-atmosphere models also exhibit some decadal dependence (Balmaseda et al. 1995; Kirtman and Schopf 1998).

A number of hypotheses have been recently proposed to explain the origin of the decadal variability in ENSO behaviour. One view is based on oceanic teleconnection, in which the subtropical SST anomalies is thought to be subducted into the equatorial thermocline, eventually affecting the equatorial SST (Gu and Philander 1997; Zhang et al. 1998). Kleeman et al. (1999) suggested that the decadal oscillation originating in the mid-latitudes may affect the equatorial SST through heat transport changes in the upper branch of the subtropical cell. Another view is based on atmospheric teleconnection proposed by Barnett et al. (1999) and Pierce et al. (2000), in which the decadal wind variability generated in the mid-latitudes extends into the tropics and forces the tropical ocean circulation.

On the other hand, relative to the ENSO timescale, the interdecadal variation may be considered as a slowly changing mean state upon which ENSO evolves. It has been recognized that the background SST and surface wind may have influence on ENSO's onset and propagation (Wang 1995). Another idea proposed by Gu and Philander (1995) emphasizes the role of secular changes in the equatorial thermocline on ENSO, as it is known that ENSO-like oscillations in intermediate coupled models are sensitive to the specific basic states of the ocean thermal structure (e.g. Zebiak and Cane 1987; Latif et al. 1997; Kirtman and Schopf 1998).

Most recently, Wang and An (2001) pointed out that from the pre-shift (1961-75) to the post-shift (1981-95) period the change of the equatorial eastern Pacific thermocline is not significant. Numerical experiments with a coupled atmosphere-ocean model illustrate that the observed changes in ENSO properties may be attributed to decadal changes in the surface winds and associated ocean surface layer dynamics without changes in the mean thermocline (Wang and An 2002). An eastward shift of the zonal wind stress anomalies with respect to the SST anomalies after 1980 was mentioned by An and Wang (2000), which appeared relevant to the increase of the ENSO period after the mid 1970s climate shift.

The joint singular value decomposition (JSVD) method (Bretherton et al. 1992), a tool for finding coupled patterns among multiple climate variables, was used by Wang and An (2001) to extract the dominant patterns derived for the 1961-75 and the 1981-95 periods, separately. The maximum SST gradient and strongest zonal wind stress anomalies were all displaced eastward by about 15 degrees during 1981-95 (Wang and An 2001); a similar result was mentioned by An and Wang (2000) using the SVD method.

Both JSVD and SVD used above are linear methods, which means the patterns for the wind stress anomalies and SST anomalies during the warm states are strictly symmetric to those during the cool states, suggesting that both the westerly and easterly anomalies will have an eastward displacement

4

after 1980. However, the atmosphere-ocean coupled mode could be nonlinear. Recently, a nonlinear canonical correlation analysis (NLCCA) method has been developed via a neural network (NN) approach (Hsieh 2000). This method has been applied to study the relation between the tropical Pacific sea level pressure (SLP) and sea surface temperature (SST) by Hsieh (2001), as well as between the surface wind stress and SST by Wu and Hsieh (2002), where the ENSO mode was found to be moderately nonlinear, with the spatial pattern for the El Niño states being considerably asymmetric to that for the La Niña states. Generally, there is a 15-20° eastward shift of the westerly anomalies during the extreme warm state relative to the easterly anomalies during the extreme cool state; while the positive SST anomalies during the warm state are located further east than the negative SST anomalies during the cool state. NLCCA was also used to study the nonlinear responses of the North American winter climate to ENSO (Wu et al. 2003).

In light of the above, the eastward shift of the equatorial westerly anomalies occurred in the late 1970s may be indicative of interdecadal changes in the nonlinearity of the ENSO mode. In this paper, the NLCCA (Hsieh 2001) model will be applied to investigate the interdecadal changes of the ENSO mode. We focus on two contrasting periods before (1961-75) and after (1981-99) the Pacific climate shift. This paper is organized as follows: In Section 2, the data and the method of NLCCA are briefly introduced. The leading NLCCA modes for the 1961-75 and 1981-99 periods were presented and compared in Section 3. The possible impact of the nonlinearity on ENSO properties was discussed in Section 4 with the delayed oscillator theory and hybrid coupled model experiments. A summary and discussion are presented in Section 5. The interdecadal changes in the nonlinearity of the ENSO mode were further verified in the Appendix by comparing the cross-validated prediction skills (from using SST to predict wind stress, and from using wind stress to predict SST) between the NLCCA and CCA models during the pre and post-shift periods.

2 Methodology and data

2.1 NLCCA

Given two sets of variables $\mathbf{x}$ and $\mathbf{y}$, canonical correlation analysis (CCA) is used to extract the correlated modes between $\mathbf{x}$ and $\mathbf{y}$ by looking for linear combinations

$$u = \mathbf{a} \cdot \mathbf{x} \quad \text{and} \quad v = \mathbf{b} \cdot \mathbf{y} \tag{1}$$

where the canonical variates u and v have maximum correlation, i.e. the weight vectors $\mathbf{a}$ and $\mathbf{b}$ are chosen such that the Pearson correlation coefficient between u and v is maximized (von Storch and Zwiers 1999).

In NLCCA, we follow the same procedure as in CCA, except that the linear combinations (from $\mathbf{x}$ to u, $\mathbf{y}$ to v) are replaced by nonlinear combinations using feed-forward neural networks (NNs), which are represented by the double-barreled NN on the left hand side of Fig. 1. By minimizing the cost function $J = -\text{cor}(\mathbf{u},\mathbf{v})$, one finds the parameters which maximize the correlation $\text{cor}(u,v)$. After the forward mapping with the double-barreled NN has been solved, inverse mappings from the canonical variates u and v to the original variables, as represented by the two standard feed-forward NNs on the right side of Fig. 1, are to be solved, where the cost function J_1 is the mean square error (MSE) of the output $\mathbf{x}'$ relative to $\mathbf{x}$ (MSE$\mathbf{x}$), and the cost function J_2, the MSE of the output $\mathbf{y}'$ relative to $\mathbf{y}$ (MSE$\mathbf{y}$) are separately minimized to find the optimal parameters for these two NNs.

The nonlinear optimization was carried out with a quasi-Newton method. To avoid the local minima problem (Hsieh and Tang 1998), an ensemble of 30 NNs with random initial weights and bias parameters was run. Also, 20% of the data was randomly selected as testing data and withheld from the training of the NNs. Runs where -cor(u,v), the MSE$\mathbf{x}$ or the MSE$\mathbf{y}$ for the testing dataset were 10% larger than those for the training dataset were rejected to avoid overfitting. The NNs with the highest cor(u,v), and smallest MSE$\mathbf{x}$ and MSE$\mathbf{y}$ was selected as the desired solution.

2.2   Data

The monthly pseudo wind stress (WS) from the Florida State University (FSU) stress analyses (Shriver and O'Brien 1995) was used in this study. The data period is January 1961 through December 1999 covering the tropical Pacific from 124°E to 70°W, 29°S to 29°N with a grid of 2° by 2°. The monthly SST came from the reconstructed historical SST data sets by Smith et al. (1996) covering the period of January 1950 to December 2000 with a resolution of 2° by 2° over the global oceans. Monthly WS and SST anomalies were calculated by subtracting the climatological monthly means, which were based on the 1961-99 period. The WS anomalies (for both zonal and meridional components) were smoothed by a 3-month running average. Linear detrending was then performed on both sets of data.

Prior to NLCCA, traditional principal component analysis (PCA), also called empirical orthogonal function (EOF) analysis, was conducted on the WS and SST anomalies over the tropical Pacific (124°E-70°W, 21°S-21°N) to compress the data into manageable dimensions and to insure that the estimated variance-covariance matrices that enter into CCA calculations can be inverted (Barnett and Preisendorfer 1987). For the WS, a combined EOF was applied to the zonal and meridional components of the WS anomalies (τ_x τ_y). Variance contributions from the 5 leading modes of WS are 15.5%, 9.8%, 6.0%, 5.2% and 3.7%, respectively, and for SST, 60.5%, 13.0%, 5.2%, 3.3% and 3.2%, respectively. The 5 leading principal components (PCs, i.e. the EOF time series) of WS and SST were used as the inputs to the NLCCA model. Fig. 2 shows the first 3 EOFs, i.e. the spatial patterns, of the SST and WS (only the zonal component is shown) and the SST. During the positive phase of the PCs, the WS EOF1 depicts a westerly anomaly patch over the central equatorial Pacific near the dateline (Fig. 2b). Within 10° of the equator, both WS EOF2 and EOF3 display a northwest-southeast contrast of the zonal WS stress anomalies (Fig. 2d and 2f). The SST EOF1 shows a typical El Niño pattern (Fig. 2a) with strong positive anomalies over the eastern equatorial Pacific. Even more concentrated SST anomalies over the eastern Pacific (off Peru) is revealed by the EOF2 (Fig.

2c), and an isolated SST anomaly over the central-eastern equatorial Pacific by the EOF3 (Fig. 2e). We will see how these patterns or their combinations will appear in the CCA or NLCCA modes in the following sections.

3 ENSO mode extracted by NLCCA

3.1 NLCCA mode 1

The 5 leading PCs of the WS and SST were divided into 2 subsets: 1961-75 and 1981-99, upon which NLCCA was conducted separately. The first NLCCA mode consists of a curve in the 5-dimension WS PC-space and another curve in the 5-dimension SST PC-space. Due to the difficulties in visualizing curves in a 5-dimension space, we focus mainly on the solutions projected onto the PC_1-PC_2 and PC_1-PC_3 planes (Fig. 3), where we can see that two curves representing the 1961-75 and 1981-99 periods are similar to each other in the PC_1-PC_2 planes except that the SST curve for 1981-99 is slightly more curved (Fig. 3a) and that the WS curve extends further to the lower-right corner (Fig. 3b) relative to the curves for 1961-75. However, the two curves in the PC_1-PC_3 plane are quite different for both SST (Fig. 3c) and WS (Fig. 3d), with one approximately flipped relative to the other along the PC_3 direction, suggesting opposite contributions of the EOF mode 3 to the NLCCA mode 1 during the 1961-75 and 1981-99 periods.

By comparing with the corresponding CCA mode (shown by the dashed and solid lines in Fig. 3), the degree of the nonlinearity of the NLCCA mode was measured. As listed in Table 1, the ratio of MSE between the NLCCA mode and the corresponding CCA mode is much smaller during 1981-99 than during 1961-75 for both SST and WS fields, and the increases of the canonical correlation and explained variance by the NLCCA mode relative to CCA mode are larger during 1981-99 than during 1961-75, indicating that the ENSO mode is more nonlinear after 1980.

8

3.2 Spatial patterns of NLCCA mode 1

For a given value of the canonical variate u, one can map from u to the 5 PCs of the SST at the output layer (of the network in the top right corner of Fig. 1). Each of the PCs can be multiplied by its associated eigenvector (i.e. the EOF spatial pattern), and the 5 modes added together gives the SST anomaly pattern for that value of u. Similarly, the WS anomaly pattern for a given value of v can be computed.

As the spatial pattern of the NLCCA mode varies along the canonical curves as displayed in Fig. 3, it is difficult to present snapshots at each time point. Here only the patterns during the minimum u and the maximum u are considered. For 1961-75, corresponding to maximum u, the SST field presents a fairly strong El Niño with positive anomalies (+2.0-2.5°C) over the central-eastern Pacific (Fig. 4c). Corresponding to minimum u, the SST field displays a La Niña with negative anomalies (about -2.0°C) over the central-western equatorial Pacific. This asymmetric SST structures between the El Niño and La Niña states were also found by Hsieh (2001) and Wu and Hsieh (2002). The WS anomaly patterns at the same time as the SST anomalies in Fig. 4a and 4c display easterly and westerly anomalies over the central-western Pacific, respectively (Fig. 4b and 4d), resembling the pattern of EOF1 (Fig. 2b). Unlike the SST, the WS field does not exhibit apparent asymmetry, implying the WS during 1961-75 was nearly linear, though the SST displayed moderate nonlinearity.

For 1981-99, the SST anomaly patterns corresponding to minimum u and maximum u (shown in Fig. 4e and 4g) are similar to those for 1961-75 except that the asymmetry between El Niño and La Niña is enhanced. The positive anomalies are intensified off the South American coast, while negative anomalies extend further west over the central-western Pacific. Also the magnitude of the SST anomalies, particularly for the positive anomalies, is increased (from +2.5°C to +3.5°C). During minimum u, the WS field presents easterly anomalies over the central-western equatorial Pacific resembling that for 1961-75 (Fig. 4b) with the amplitude somewhat strengthened. The WS field during maximum u

displays further intensified westerly anomalies over the central Pacific (Fig. 4h), shifted eastward by about $25°$ and southward by about $5°$ relative to the easterly anomalies in Fig. 4f. With easterly anomalies over the western equatorial Pacific, the pattern in Fig. 4h is actually a combination of patterns from WS EOF1, -EOF2 and EOF3 (Fig. 2b, 2d and 2f). The asymmetry of the zonal WS structure between Fig. 4f and 4h indicates that the WS field is quite nonlinear during the 1981-99 period.

Our results here are basically consistent with those of Hsieh (2001), where NLCCA was applied to the SLP and SST data for 1950-99. It was pointed by Hsieh (2001) that, during 1950-75, the SLP showed no nonlinearity, while the SST revealed weak nonlinearity. During 1976-99, the SLP displayed weak nonlinearity, while the weak nonlinearity in the SST was further enhanced. Our results also agree with the linear SVD analysis of Wang and An (2001), where a $15°$ longitude eastward displacement of WS anomalies was found, which is basically an average of the patterns shown in Fig. 4f and 4h.

In Fig. 3a, on either curve, both large positive and negative SST PC_1 concur with positive SST PC_2. In Fig. 3b, both large positive and negative WS PC_1 concur with large negative WS PC_2. Considering the EOF1 and EOF2 of SST and WS, we can see this PC_1-PC_2 combination facilitates the asymmetry of SST and WS anomaly pattern illustrated in Fig. 4. Then why did the WS have very weak nonlinearity during 1960-75 but have considerable nonlinearity during 1981-99? The NLCCA curve for the 1981-99 WS (shown as squares in Fig. 3b) extends to larger negative PC_2 is one explanation. In addition, note that in Fig. 3d the two curves are flipped along the PC_3 direction. For 1981-99, large positive WS PC_1 concurs with large positive PC_3 (upper-right corner), which supports the eastward and slightly southward shift of the westerly anomalies (see the WS EOF3 pattern in Fig. 2f), further intensifying the asymmetry generated by the nonlinear PC_1-PC_2 combination. However, for 1961-75, large positive WS PC_1 concurs with negative PC_3 (lower-right corner), which does not intensify the asymmetry. The two curves are close to each other with small PC_3 values when PC_1 is negative (Fig.

3d), suggesting that the WS patterns (easterly anomalies) during La Niña states should be similar during 1961-75 and 1981-99, as can be seen in Fig. 4b and 4f.

In Fig. 3c, on the curve for 1981-99, large negative SST PC_1 concurs with large positive SST PC_3, which intensifies the negative anomalies over the central equatorial Pacific, as over there is a negative anomaly in the SST EOF3 (Fig. 2e), thus enhancing the asymmetry of SST between El Niño and La Niña. In contrast, on the curve for 1961-75, large negative SST PC_1 concurs with large negative SST PC_3, which weakens the negative anomalies over the central equatorial Pacific, reducing the nonlinearity of SST.

Therefore, the difference in the nonlinear combination between PC_1 and PC_3 indicates the inter-decadal changes of the ENSO mode. As the WS PC_3 has a similar amplitude as the WS PC_2, while the SST PC_3 is much weaker than the SST PC_2, the interdecadal changes in the WS are more pronounced than in the SST.

Comparing Fig. 4h and Fig. 4d, we note that the presence of easterly anomalies near the western equatorial boundary in the 1981-99 period but not in the 1961-75 period. Easterly anomalies near the western boundary play an important role in the western Pacific oscillatory mechanism of Weisberg and Wang (1997). Hence the NLCCA result is consistent with an enhanced western Pacific oscillator in the 1981-99 period. Intriguingly, during La Niña, even for the 1981-99 period, there is no corresponding westerly anomalies near the western boundary (Fig. 4f).

For comparison, spatial patterns for the CCA mode 1 are displayed in Fig. 5. For either 1961-75 or 1981-99, the SST anomaly patterns corresponding to minimum u and maximum u are completely symmetric, i.e., mirror images except for some difference in magnitude, as are the WS fields. While the SST and WS anomaly patterns for CCA mode 1 during the 1961-75 period are similar to those during 1981-99, with both roughly resembling the patterns of EOF1 (Fig. 2a and 2b), we still can see an eastward displacement of the anomaly patterns for 1981-99 relative to those for 1961-75, although

11

the displacement is not as dramatic as that shown in Fig. 4. Also the SST or WS anomalies for 1981-99 are somewhat stronger than those for 1961-75 (Fig. 5). For cross-validated comparisons between NLCCA and CC, see the Appendix.

4   Nonlinearity and the ENSO period

4.1   Delayed oscillator theory

The dominant period of ENSO was increased from 2-3 years during the 1960s and 1970s to 4-5 years during the 1980s and 1990s (Wang and Wang 1996). One possible explanation for this is the eastward shift of the westerly anomalies after 1980 (An and Wang 2000; Wang and An 2001). Let us examine the consequences based on the delayed oscillator theory (Suarez and Schopf 1988): Let L be the width of the equatorial Pacific Ocean, and x the distance between the center of the westerly wind anomaly and the eastern boundary. If the wind anomaly appears at time $t = 0$, then warm SST appears at the eastern boundary at time $t_1 = x/c_K$, with c_K the eastward Kelvin wave speed. A cool Rossy wave also propagates westward at speed c_R for a distance of $L - x$ until it reflects at the western boundary as a cool eastward propagating Kelvin wave. The warming at the eastern boundary stops when the cool Kevin wave finally arrives at time $t_2 = (L - x)/c_R + L/c_K$. Hence the duration of warming at the eastern boundary is

$$T = t_2 - t_1 = (L - x) \left(\frac{1}{c_R} + \frac{1}{c_K} \right) . \tag{2}$$

This implies that an eastward shift in the wind anomaly, i.e. a decrease in x, leads to an increase in T.

If x_A and x_B denote respectively the values of x before and after the climate shift, and T_A and T_B denote the corresponding durations of warming, then

$$\frac{\Delta T}{T_A} \equiv \frac{T_B - T_A}{T_A} = \frac{x_A - x_B}{L - x_A} . \tag{3}$$

12

Note that the result is independent of the actual values of the Kelvin and Rossby wave speeds, provided they did not change significantly over the two periods. If we assume the western boundary is at 124°E, and x_A is at the dateline, and $x_A - x_B$ to be 25°, then $\Delta T/T_A$ is 45%. Since the 25° shift in the westerly anomaly is based on the extreme of the NLCCA mode, while the average warm event may not reach the extreme, so an average shift may only be about 20°, which would still give a $\Delta T/T_A$ of 36%. We shall later see that these rough estimates for the fractional lengthening of the warm events as derived from the simple delayed oscillator theory actually agree quite well with the estimates from our hybrid coupled model.

For the linear JSVD, SVD or CCA results, the pattern of the easterly anomalies during the La Niña states is strictly symmetric to that of westerly anomalies during the El Niño states, i.e. the easterly anomaly fetch will occur over the same location where the westerly anomaly fetch takes place. Hence, the durations for both warm and cool events will be prolonged by the same amount, as can be seen in the wavelet diagram (An and Wang 2000, Fig. 1), where both positive and negative centers shift towards lower frequency after 1980.

However, our NLCCA results indicate that the coupled mode in the tropical Pacific could be nonlinear. The patterns for WS or SST anomalies could be very asymmetric, e.g. during the period 1981-99, only the westerly anomalies shifted eastward, while the easterly anomalies basically remained over the dateline. Thus, we argue that only the duration of warm events is prolonged, while that of cool events is unchanged.

4.2 Hybrid coupled model experiments

The statistical atmospheric model is based on the first mode of the NLCCA or the CCA, which estimates the WS anomalies using the SST anomalies as predictors. The ocean model is basically that used in the Lamont model (Zebiak and Cane 1987). It is an anomaly model with the climatology

of SST, currents, thermocline depth and background wind prescribed. The coupling procedure is as following: The SST anomalies from the ocean model are projected onto the eigenvectors of the observed SST anomalies (Fig. 2) yielding the 5 leading PCs of SST, which are served as the inputs to the NLCCA or CCA model. The outputs of the NLCCA or CCA model are the 5 PCs of the WS, which are multiplied by the corresponding eigenvectors (Fig. 2) to generate the WS anomalies. The WS anomalies are then used to force the ocean model to predict new SST anomalies. The above procedure is repeated until a desired integration is completed. Before running the coupled model, the ocean model has been spun up with westerly anomalies for a certain time. It is worth pointing out that the FSU pseudo wind stress $\vec{\tau} = \vec{V} \cdot |\vec{V}|$ (with a unit of m^2/s^2) must be converted to real stress (with unit dyne) for coupling by multiplying it by a coefficient $\mu = \rho C_D$, where ρ is the air density and C_D is the drag coefficient. In the following coupled model experiments, μ may be considered as a coupling coefficient.

Based on the data for 1961-75 and 1981-99, 2 NLCCA models and 2 corresponding CCA models were built. Having the 4 statistical atmospheric models coupled with the ocean model, we consequently have 4 HCMs, named as HCM_{NL6175}, HCM_{NL8199}, HCM_{L6175} and HCM_{L8199}, respectively. Each HCM was run 250 years and the simulations for the last 150 years were used for analysis. Fig. 6 presents the Niño3 indices obtained from the last 50-year integrations by the 4 HCMs with a coupling coefficient $\mu = 0.05$. The power spectrum analysis shows that the dominant periods for the simulated SST oscillations by HCM_{L6175}, HCM_{NL6175}, HCM_{L8199} and HCM_{NL8199} are 27.3, 24.0, 28.6 and 37.8 months, respectively. It is notable that the period is significantly increased by using HCM_{NL8199} (Fig. 6d), confirming that nonlinearity may prolong the ENSO period. In fact, because of the weak nonlinearity during 1961-75, the oscillation period from the HCM_{NL6175} has not increased relative to that of HCM_{L6175}.

Contrast to the regular SST oscillations simulated by the other 3 HCMs, the HCM_{NL8199} presents

an oscillation with considerable irregularity and somewhat enhanced amplitudes (up to $+4°C$) (Fig. 6d). The $HCM_{NL81199}$ model also shows that multi-year El Nino events are possible. The duration of the warm phases is apparently increased in Fig. 6d relative to other 3 panels, while the duration of cool phases remains basically unchanged (see Table 2). Therefore, the prolongation of the model ENSO period is mainly due to the increased duration of its warm phase.

A series of sensitivity experiments of the 4 HCMs were conducted by varying the coupling coefficient μ from 0.030 to 0.075 by steps of 0.005. We found that, all 4 models can produce stable oscillations when $\mu > 0.04$, otherwise the initial fluctuations were damped quickly. However, for the HCM_{NL8199}, too large a μ (> 0.07) leads to a climate drift with the Niño3 index varying between $+2$ and $+3.5°C$ (figure not shown). Excluding these extreme μ regimes, the model ENSO period is not very sensitive to the change of μ (see Table 3), confirming the robustness of our results.

5   Summary and discussion

Following the abrupt North Pacific climate shift in the mid 1970s, the period, amplitude, spatial structure, and temporal evolution of El Niño notably changed. In this study, the NLCCA model was used to extract the coupled mode between the tropical Pacific wind stress and sea surface temperature during the 1961-75 period and the 1981-99 period. From the leading NLCCA mode, we found notable interdecadal dependence in the nonlinearity of the coupled mode. During 1961-75, the WS showed no nonlinearity, while the SST revealed some nonlinearity. During 1981-99, the WS displayed fairly strong nonlinearity, and the nonlinearity in the SST was further enhanced. While nonlinearity can be detected between the EOF PC_1 and PC_2 as well as PC_1 and PC_3, the nonlinearity between PC_1 and PC_3 counteracts the nonlinearity between PC_1 and PC_2 in 1961-75, but reinforces the nonlinearity between PC_1 and PC_2 in 1981-99, resulting in greater nonlinearity during the 1981-99 period.

An advantage of the NLCCA over the CCA is that NLCCA is capable of presenting the asymme-

try between the El Niño states and La Niña states. For the SST of both periods, negative anomalies during La Niña are centered further west of the positive anomalies during El Niño. The displacement is enhanced during 1981-99 as the main warming occurred even further east (off the South American coast). For the WS of the period 1961-75, the easterly anomaly patch during La Niña is basically symmetric to the westerly anomaly patch during El Niño with both centers located over the dateline. For the WS of the period 1981-99, the easterly anomalies during La Niña are intensified but unmoved, while the westerly anomalies during El Niño are shifted eastward by about 25° with increased amplitude. That the asymmetry between El Niño and La Niña was enhanced after 1980 (especially in the WS) suggests an increase in the nonlinearity of the ENSO mode.

To further assess the interdecadal changes in the nonlinearity of ENSO mode, simple forecast models based on the NLCCA or CCA mode 1 were designed to predict the SST (using the simultaneous wind stress as predictor) and the WS (using the simultaneous SST as predictor). Comparable prediction skills (in terms of cross-validated correlation and root mean square error) are obtained by the NLCCA and CCA models during 1961-75, while significant improvement of the NLCCA model relative to the CCA model is found during 1981-99, confirming that the ENSO mode has greater nonlinearity after 1980 (see Appendix for details).

The linearity of traditional CCA (or SVD) forces both westerly and easterly anomalies to shift eastward after 1980. According to the delayed oscillator theory, the ENSO period will increase as the duration for both the warm phase and that for the cool phase are prolonged. However, the NLCCA mode demonstrates that only the westerly anomalies shifted eastward after 1980. Thus we argue that the increase of the ENSO period after 1980 is mainly due to the prolongation of the warm phase. This was verified by numerical experiments with a hybrid coupled model (HCM), which combines the statistical atmospheric model (based on the NLCCA or CCA mode 1) and an intermediate dynamic ocean model (the Lamont ocean model).

16

In our HCMs for different decades, the annual climatological fields for the ocean model (e.g. the mean currents and upwelling) and the wind fields were kept unchanged, allowing us to focus on the changes of the anomaly mode. However, the changes in the climatological states may also lead to the changes in the ENSO propagation (Wang and An 2002). This explains why we did not see apparent interdecadal changes of ENSO propagation in our numerical experiments. As a matter of fact, an important implication of prolonging the warm phase of ENSO is a warmer mean state, especially in the eastern equatorial Pacific.

In the delayed oscillator theory, the ENSO period depends on not only the zonal position of the wind patch but also the meridional structure of the equatorial wave packet and the reflectivity at the western boundary. In this paper, we only emphasized the zonal position of the wind stress patch. In addition to the delayed oscillatior theory, several other machanisms, such as the western Pacific oscillator paradigm (Weisberg and Wang 1997), the equatorial ocean recharge paradigm (Jin 1997) and stochastic forcing may have effects on the ENSO properties.

Acknowledgements

Appendix: Cross-validation for the NLCCA model

Once the weight parameters (in the NN of Fig. 1) have been determined, an NLCCA model is built, the standard deviation $\text{std}(u)$ and $\text{std}(v)$ are known, and $\langle u \rangle = \langle v \rangle = 0$. If new $\mathbf{x}$ data become available,

17

then u can be calculated, and v estimated by $u \cdot \text{std}(v)/\text{std}(u)$, which can then be used to predict $\mathbf{y}$. Similarly, $\mathbf{x}$ can be predicted using new $\mathbf{y}$ data.

For cross validation, we divided the data for 1961-75 period into 3 segments of equal length (5 years). Three NLCCA models were to be built. The first was built without the data of the 1st segment, which was to be used as independent validation (or testing) data. Similarly, the 2nd and the 3rd models had the 2nd and 3rd segment of data left out for independent validation, respectively. Independent predictions by the 3 models were then collected to form a data time series of the whole period from 1961 to 1975, which was then compared with the observed data to alleviate the prediction skill. Same procedures were done on the data for 1981-99. Here we simply focus on the predictions of zero lead time, i.e. predict the WS using the simultaneous SST as predictor, and predict the SST using the simultaneous WS as predictor. Also only the NLCCA or CCA mode 1 is used here.

A.1 For the WS

Fig. 7 shows the time evolution of the zonal WS anomalies along the equator (averaged within 5°S-5°N) predicted by the NLCCA models, where the westerly (easterly) anomalies associated with major El Niño (La Niña) events during the past 4 decades are successfully reproduced. It is notable that the zonal WS anomalies, especially the westerly anomalies, are intensified during the 1981-99 period. In Fig. 7b, an eastward displacement between the westerly (positive) anomalies and easterly (negative) anomalies can still be seen, although the displacement is much smaller than that shown in Fig. 4f and 4h. In contrast, there is basically no displacement between the westerly and easterly anomalies in the predictions for 1961-75 (Fig. 7a).

Geographical distributions of the prediction skill for the zonal and meridional WS anomalies by the NLCCA models are shown in Fig. 8. For the zonal WS, the higher correlation is located over the central-western equatorial Pacific, and the NLCCA models have higher correlation skill in 1981-99

18

than in 1961-75 (Fig. 8a and 8b). Also shown in Fig. 8 are the difference between the skill of NLCCA models and the corresponding CCA models (NLCCA minus CCA), where significant improvement of the correlation (0.3-0.4) occurs in 1981-99 over the central-eastern Pacific and the western Pacific (Fig. 8d), while there is little improvement for 1961-75 (Fig. 8c). For the meridional WS, higher NLCCA skill relative to the CCA skill also occurs in the 1981-99 period over the central equatorial Pacific (Fig. 8h), versus insignificant improvement in the 1961-75 period (Fig. 8g). Similar conclusions are reached when examining the root mean square error (RMSE) (not shown).

That the NLCCA models exhibit more advantage over the CCA models during the 1981-99 period than during the 1961-75 period indicates that the ENSO mode is more nonlinear after 1980, confirming the results described in Section 3.

A.2 For the SST

Fig. 9 shows the time evolution of the equatorial SST anomalies (averaged within 5°S-5°N) predicted by the NLCCA models. Compared to the observation, despite the relative weak amplitudes, the SST anomalies during the past 4 decades are well predicted even with one NLCCA mode. The asymmetry between El Niño and La Niña, i.e. the eastward shift between the warming and the cooling is also successfully reproduced. This shift is more significant during 1981-99 (Fig. 9b) than during 1961-75 (Fig. 9a), suggesting again that there is more nonlinearity in the ENSO mode after 1980.

Table 4 lists the correlations and RMSE between the observed and predicted SST anomalies averaged over Niño12 (90°W-80°W, 10°S-0°), Niño3 (150°W-90°W, 5°S-5°N), Niño3.4 (170°W-120°W, 5°S-5°N) and Niño4 (160°E-150°W, 5°S-5°N) areas. During the period 1961-75, the NLCCA and CCA models have comparable prediction skills over all 4 areas. During 1981-99, despite similar skills over the Niño3.4 and Niño3 areas, significant improvement of prediction skills between the NLCCA and CCA models is achieved over the Niño4 and Niño12 areas. Note that, during 1981-99, the Niño12 area

19

is where strong warming occurred (Fig. 4g), and the Niño4 area, where strong cooling occurred (Fig. 4e). SST anomalies over these 2 areas cannot be well described by the CCA model. It is natural that the NLCCA models give better prediction skills over these 2 areas.

References

An S-I, Wang B (2000) Interdecadal changes of the structure of the ENSO mode and its impact on the ENSO frequency. J Clim 13:2044-2055

Balmaseda MA, Davet K, Anderson DLT (1995) Decadal and seasonal dependence of ENSO prediction skill. J Clim 8:2705-2715

Barnett TP, Preisendorfer R (1987) Origins and levels of monthly and seasonal forecast skill for United States surface air temperatures determined by canonical correlation analysis. Mon Weather Rev 115:1825-1850

Barnett TP, Pierce DW, Latif M, Dommenget D (1999) Interdecadal interactions between the tropics and midlatitudes in the Pacific basin. Geophys Res Lett 26:615-618

Bretherton CS, Smith C, Wallace JM (1992) An intercomparison of methods for finding coupled patterns in climate data. J Clim 5:541-560

Gu D, Philander SGH (1995) Secular changes of annual and interannual variability in the tropics during the past century. J. Clim 8:864-876

Gu D, Philander SGH (1997) Interdecadal climate fluctuations that depend on exchanges between the tropics and extratropics. Science 275:805-807

Hsieh WW, Tang B (1998) Applying neural network models to prediction and data analysis in meteorology and oceanography. Bull. Amer. Meteor. Soc. 79:1855-1870

Hsieh WW (2000) Nonlinear canonical correlation analysis by neural networks. Neural Networks 13:1095-1105

Hsieh WW (2001) Nonlinear canonical correlation analysis of the tropical Pacific climate variability using a neural network approach. J Clim 14:2528-2539

Jin FF (1997) An equatorial ocean recharge paradigm for ENSO, Part 1: Conceptual Model. J Atmos Sci 54: 811-829

Kirtman BP, Schopf PS (1998) Decadal variability in ENSO predictability and prediction. J. Clim 11: 2804-2822

Kleeman R, McCreary JP, Klinger BA (1999) A mechanism for generating ENSO decadal variability. Geophys. Res. Lett. 26: 1743-1746

Latif M, Kleeman R, Eckert C (1997) Greenhouse warming, decadal variability, or El Niño? An attempt to understand the anomalous 1990s. J Clim 10: 2221-2239

Pierce DW, Barnett TP, Latif M (2000) Connections between the Pacific ocean tropics and midlatitudes on decadal time scales. J Clim 13:1173-1194

Rasmusson EM, Carpenter TH (1982) Variations in tropical sea surface temperature and surface wind fields associated with the Southern Oscillation/ El Niño. Mon Weather Rev 110:354-384

Suarez MJ, Schopf PS (1988) A delayed oscillator for ENSO. J. Atmos Sci 45:3283-3287

Shriver JF, O'Brien JJ (1995) Low frequency variability of the equatorial Pacific ocean using a new pseudostress dataset: 1930-1989. J Clim 8:2762-2786.

Smith TM, Reynolds RW, Livezey RE and Stokes DC (1996) Reconstruction of historical sea surface temperatures using empirical orthogonal functions. J Clim 9:1403-1420

Trenberth KE (1990) Recent observed interdecadal climate changes in the Northern Hemisphere. Bull Amer Meteor Soc 71:988-993

Trenberth KE, Hurrell JW (1994) Decadal atmosphere-ocean variations in the Pacific. Clim Dyn 9:303-319

von Storch H, Zwiers FW (1999) *Statistical Analysis in Climate Research. Cambridge*, Cambridge Univ Pr 484 pp

Wallace JM, Rasmusson EM, Mitchell T, Kousky V, Sarachik E, von Storch H (1998) On the structure and evolution of ENSO-related climate variability in the tropical Pacific: Lessons. J Geophys Res 103:14241-14259

Wang B (1995) Interdecadal changes in El Niño onset in the last four decades. J Clim 8:267-285

Wang B, Wang Y (1996) Temporal structure of the Southern Oscillation as revealed by waveform and wavelet analysis. J Clim 9:1586-1598

Wang B, An S-I (2001) Why the properties of El Niño changed during the late 1970s. Geophys Res Lett 28:3709-3712

Wang B, An S-I (2002) A mechanism for decadal changes of ENSO behavior: roles of background wind changes. Clim Dyn 18:475-486

Weisberg, RH, Wang C (1997) A western Pacific oscillator paradigm for the El Niño-Southern Oscillation. Geophy Res Lett 24:779-782

Wu A, Hsieh WW (2002) Nonlinear canonical correlation analysis of the tropical Pacific wind stress and sea surface temperature. Clim Dyn 19: 713-722

Wu A, Hsieh WW, Zwiers FW (2003) Nonlinear modes of North American winter climate variability derived from a general circulation model simulation. 16: 2325-2339

Zhang R-H, Rothstein LM, Busalacchi AJ (1998) Origin of upper ocean warming and El Niño change

    on decadal scales in the tropical Pacific Ocean. Nature 391:879-883

Zebiak SE, Cane MA (1987) A model El Niño-Southern Oscillation. Mon Weather Rev 115:2262-2278

Table 1: Statistics of the NLCCA mode 1 and the corresponding CCA mode 1 for the 1961-75 and 1981-99 periods. R_{SST} represents ratio between the mean square error (MSE) of the NLCCA mode 1 and that of the corresponding CCA mode 1 for SST, and R_{WS} for WS. A ratio of 1 would indicate no difference between the NLCCA and CCA modes, while a small ratio indicates strong nonlinearity. Corr(u,v) denotes the canonical correlation coefficient, and EVP_{SST}, the explained percentage of the total variance by the NLCCA mode 1 for the SST, and EVP_{WS} for the WS, with the difference (NLCCA minus CCA) given in parenthesis.

	1961-75	1981-99
R_{SST}	0.894	0.777
R_{WS}	0.947	0.754
corr(u,v)	0.957 (+0.009)	0.975 (+0.02)
EVP_{SST}	64.2% (+1.7%)	63.6% (+6.7%)
EVP_{WS}	17.2% (+1.5%)	21.5% (+6.1%)

Table 2: Dominant period (in months) of the Niño3 indices simulated by the hybrid coupled models with the coupling coefficient $\mu = 0.05$. Also shown are the mean duration of warm phase and cool phase within one period.

	1961-75			1981-99		
	period	warm phase	cool phase	period	warm phase	cool phase
L	27.3	20.2	7.1	28.6	21.0	7.6
NL	24.0	16.0	8.0	38.7	30.9	7.8

Table 3: Dominant period (in months) of the Niño3 indices simulated by the four hybrid coupled models with the coupling coefficient μ varying from 0.04 to 0.075. '−' means the model SST oscillations were damped or drifted unrealistically.

μ	HCM_{L6175}	HCM_{NL6175}	HCM_{L8199}	HCM_{NL8199}
0.040	26.7	24.0	−	−
0.045	27.3	24.1	28.5	36.7
0.050	27.3	24.0	28.6	38.7
0.055	26.5	24.3	29.0	37.3
0.060	26.5	25.6	30.0	37.6
0.065	26.9	26.2	30.0	38.5
0.070	27.3	26.3	31.2	−
0.075	27.7	26.7	31.4	−

Table 4: Cross-validated correlation skill (corr) and RMSE (in °C) of the predicted SST anomalies by the NLCCA models (only the first mode was used) relative to the observations over the Niño12, Niño3, Niño3.4, and Niño4 areas. The difference between the NLCCA and the corresponding CCA model (NLCCA minus CCA) is shown in parenthesis.

	corr 1961-75	corr 1981-99	RMSE 1961-75	RMSE 1981-99
Niño4	0.59 (+0.03)	0.79 (+0.11)	0.48 (-0.02)	0.27 (-0.11)
Niño3.4	0.84 (0.00)	0.86 (-0.01)	0.45 (-0.01)	0.46 (+0.03)
Niño3	0.84 (+0.01)	0.79 (0.00)	0.48 (0.00)	0.59 (-0.01)
Niño12	0.69 (+0.01)	0.71 (+0.16)	0.66 (-0.03)	0.78 (-0.23)
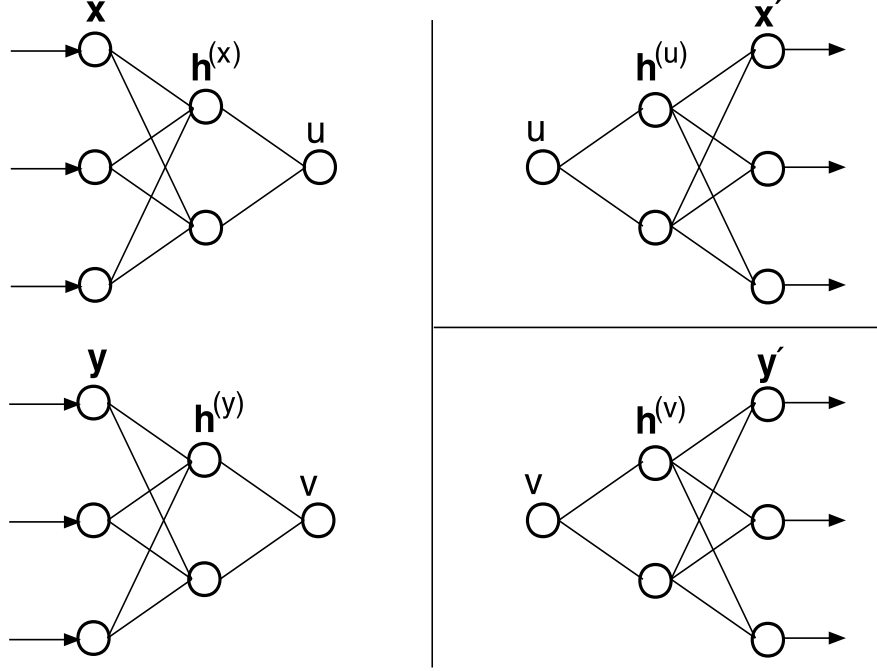
Figure 1: A schematic diagram illustrating the three feed-forward neural networks (NN) used to perform the NLCCA model of Hsieh (2001). The double-barreled NN on the left maps from the inputs $\mathbf{x}$ and $\mathbf{y}$ to the canonical variates u and v. Starting from the left, there are l_1 input $\mathbf{x}$ variables ('neurons' in NN jargon), denoted by circles. The information is then mapped to the next layer (to the right)— a 'hidden' layer $\mathbf{h}^{(x)}$ (with l_2 neurons). For input $\mathbf{y}$, there are m_1 neurons, followed by a hidden layer $\mathbf{h}^{(y)}$ (with m_2 neurons). The mappings continue onto u and v. The cost function J forces the correlation between u and v to be maximized, and by optimizing J, the weights (i.e. parameters) of the NN are solved. On the right side, the top NN maps from u to a hidden layer $\mathbf{h}^{(u)}$ (with l_2 neurons), followed by the output layer $\mathbf{x}'$ (with l_1 neurons). The cost function J_1 minimizes the MSE($\mathbf{x}$), the mean square error of $\mathbf{x}'$ relative to $\mathbf{x}$. The third NN maps from v to a hidden layer $\mathbf{h}^{(v)}$ (with m_2 neurons), followed by the output layer $\mathbf{y}'$ (with m_1 neurons). The cost function J_2 minimizes the MSE($\mathbf{y}$), the MSE of $\mathbf{y}'$ relative to $\mathbf{y}$. When applied to the tropical Pacific, the $\mathbf{x}$ inputs were the first 5 principal components (PCs) of the SST field, the $\mathbf{y}$ inputs, the first 5 PCs of the wind stress, and the number of hidden neurons were $l_2 = m_2 = 3$. An ensemble of 30 trials with random initial weights were run. Among all these runs, the one with the highest cor(u,v), and smallest MSE$\mathbf{x}$ and MSE$\mathbf{y}$ was selected as the desired solution.
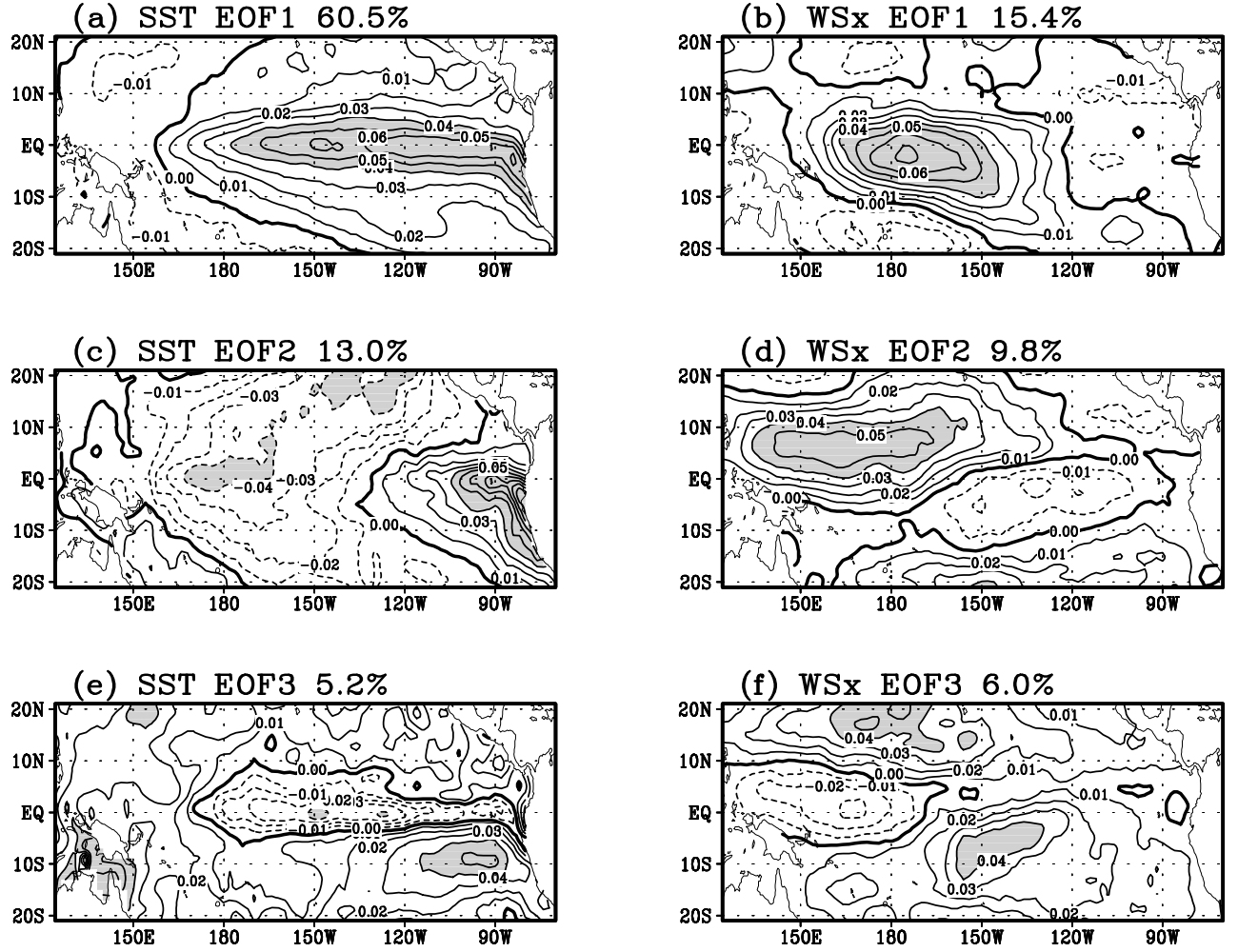
Figure 2: The first 3 EOFs of the tropical Pacific SST anomalies (left column) and WS anomalies (right column, only the zonal component is shown). Solid curves denote positive contours, dashed curves, negative contours, and thick curves, zero contours. The contour interval is 0.01. The EOFs have been normalized to unit norm. Areas with values greater than 0.04 or less than -0.04 are shaded.
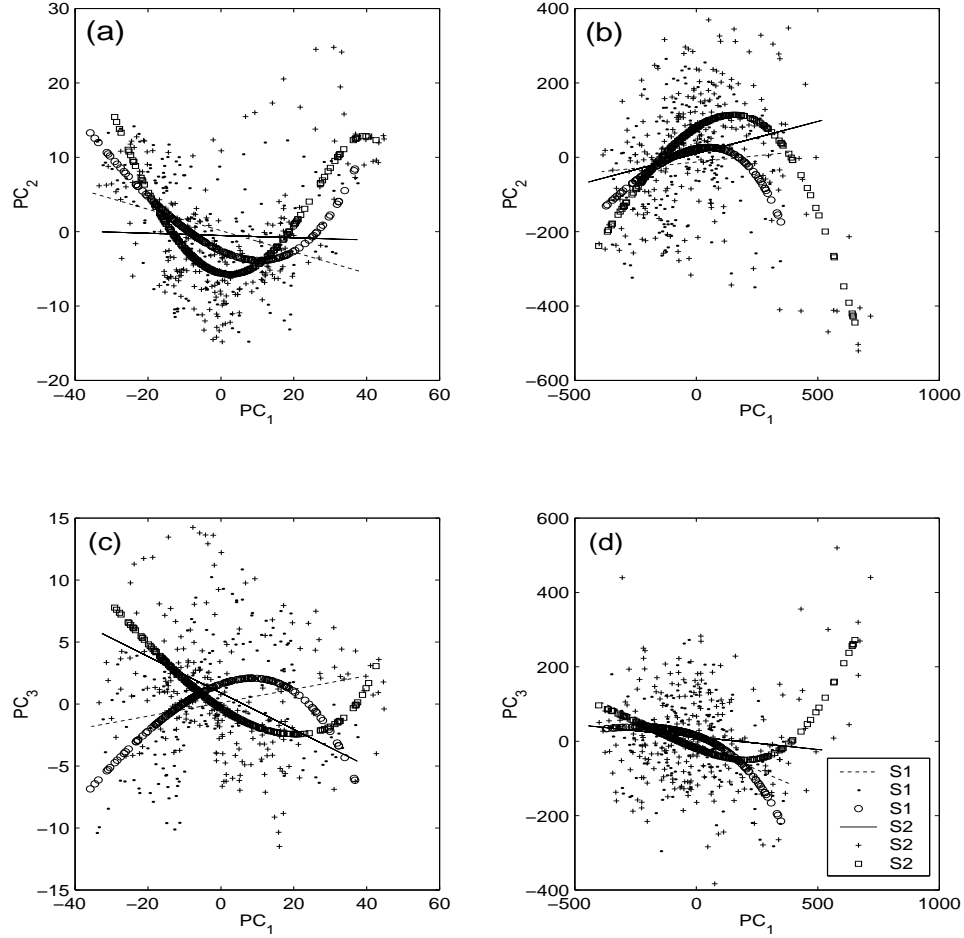
Figure 3: The first NLCCA mode of the tropical Pacific SST (left column) and wind stress (WS) anomalies (right column) projected onto the PC_1-PC_2 planes shown in panels (a) and (b), and onto the PC_1-PC_3 planes shown in panels (c) and (d), respectively. The data for the period 1961-75 (data subset S1) are denoted by dots, for the period 1981-99 (data subset S2), by the symbol '+'. The projected NLCCA solutions for 1961-75 and 1981-99 are denoted by the circles and squares. respectively. The corresponding CCA mode 1 is shown by the dashed line (1961-75) and solid line (1981-99).
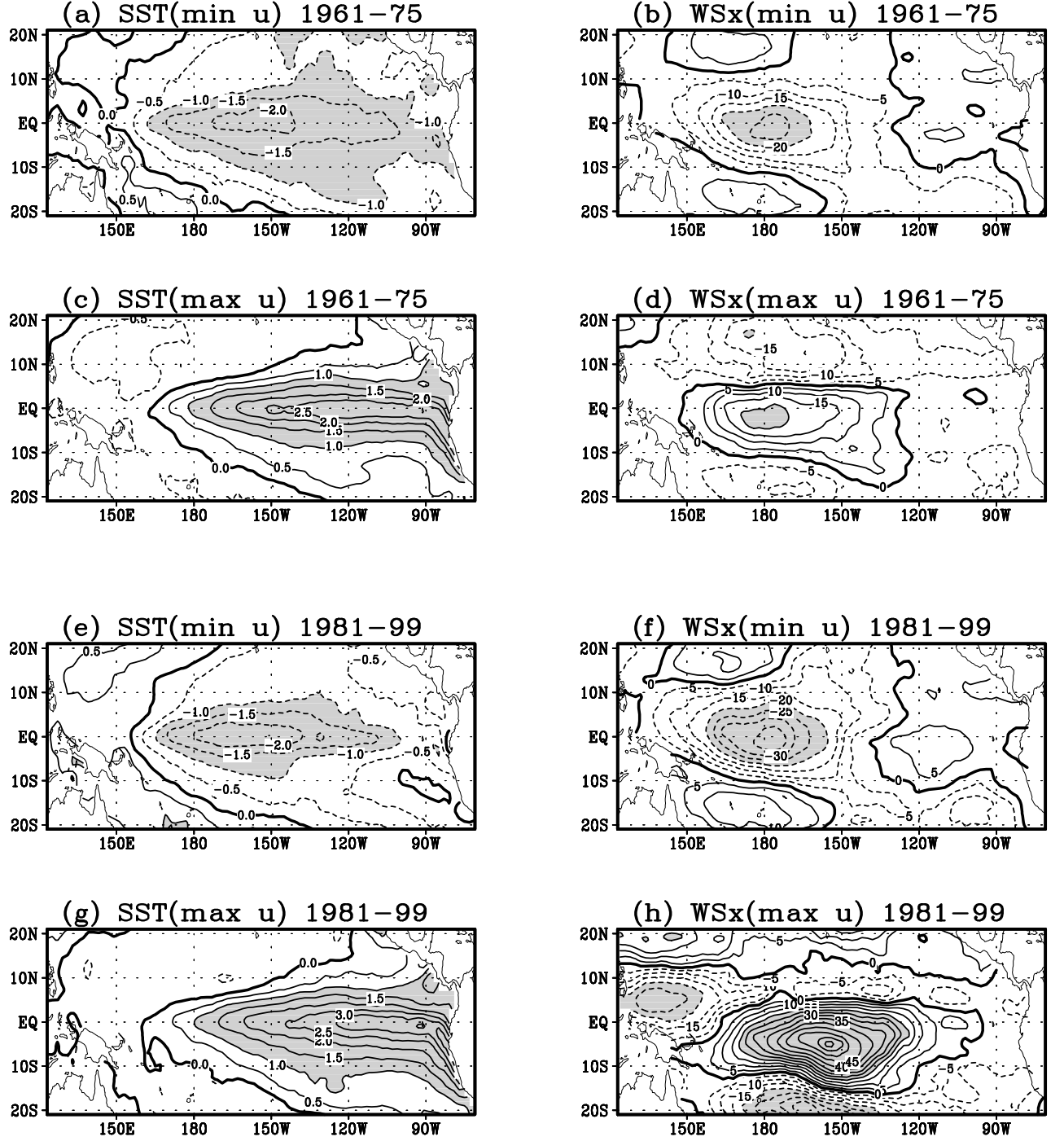
Figure 4: The SST anomaly patterns (left column) and WS anomaly patterns (right column) from the NLCCA mode 1 when the canonical variate u taking its minimum (panels a, b, e and f) and maximum values (panels c, d, g, and h). The upper 4 panels represent the period 1961-75, and lower 4 panels, the period 1981-99. The contour interval is 0.5°C for the SST anomalies, and 5 m^2/s^2, for the WS anomalies. Areas where the SST anomalies are larger than +1°C or less than -1°C, or the WS anomalies are larger than +20m^2/s^2 or less than -20m^2/s^2 are shaded. For WS, solid contours indicate westerly anomalies, and dashed contours, easterly anomalies.
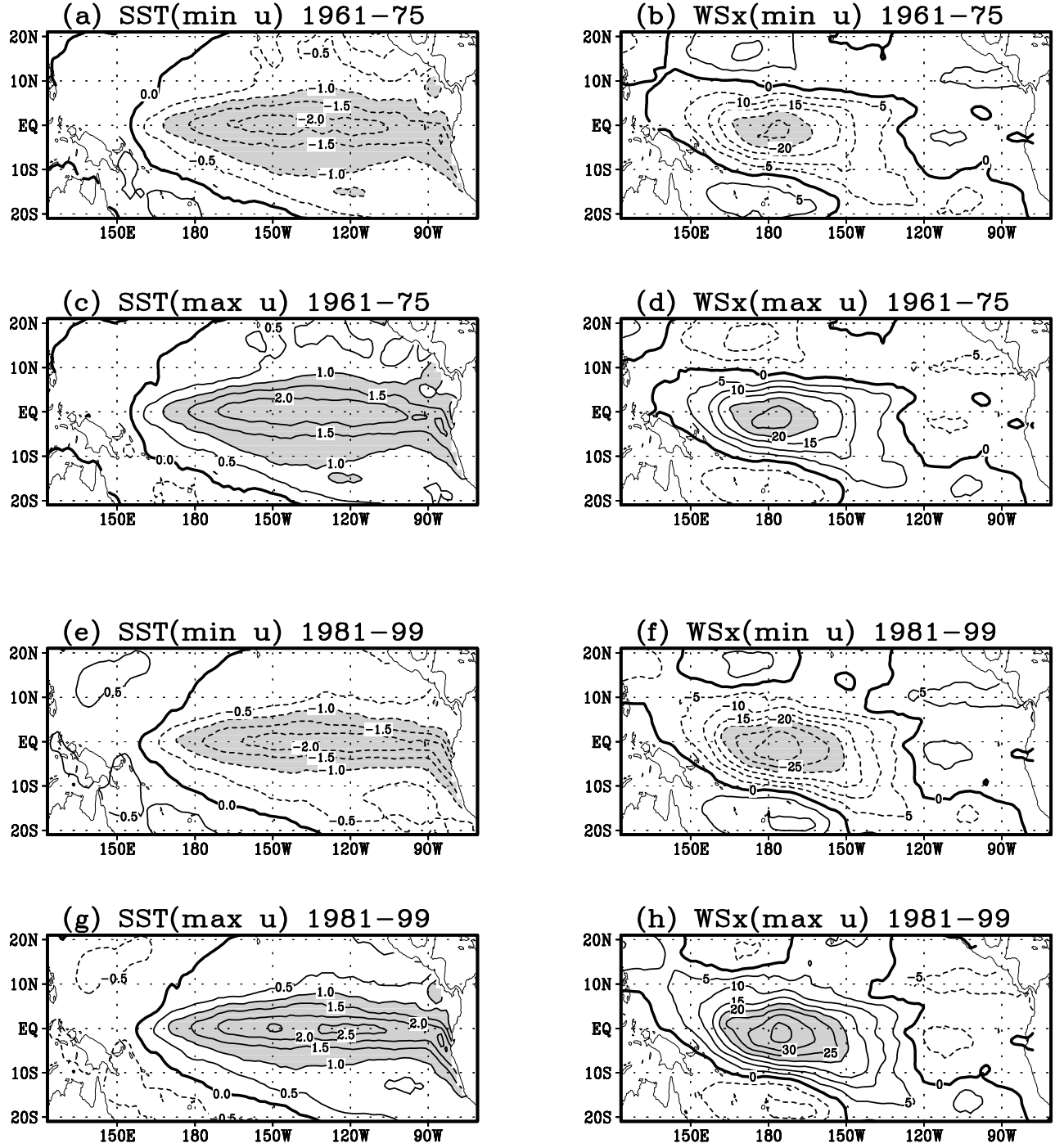
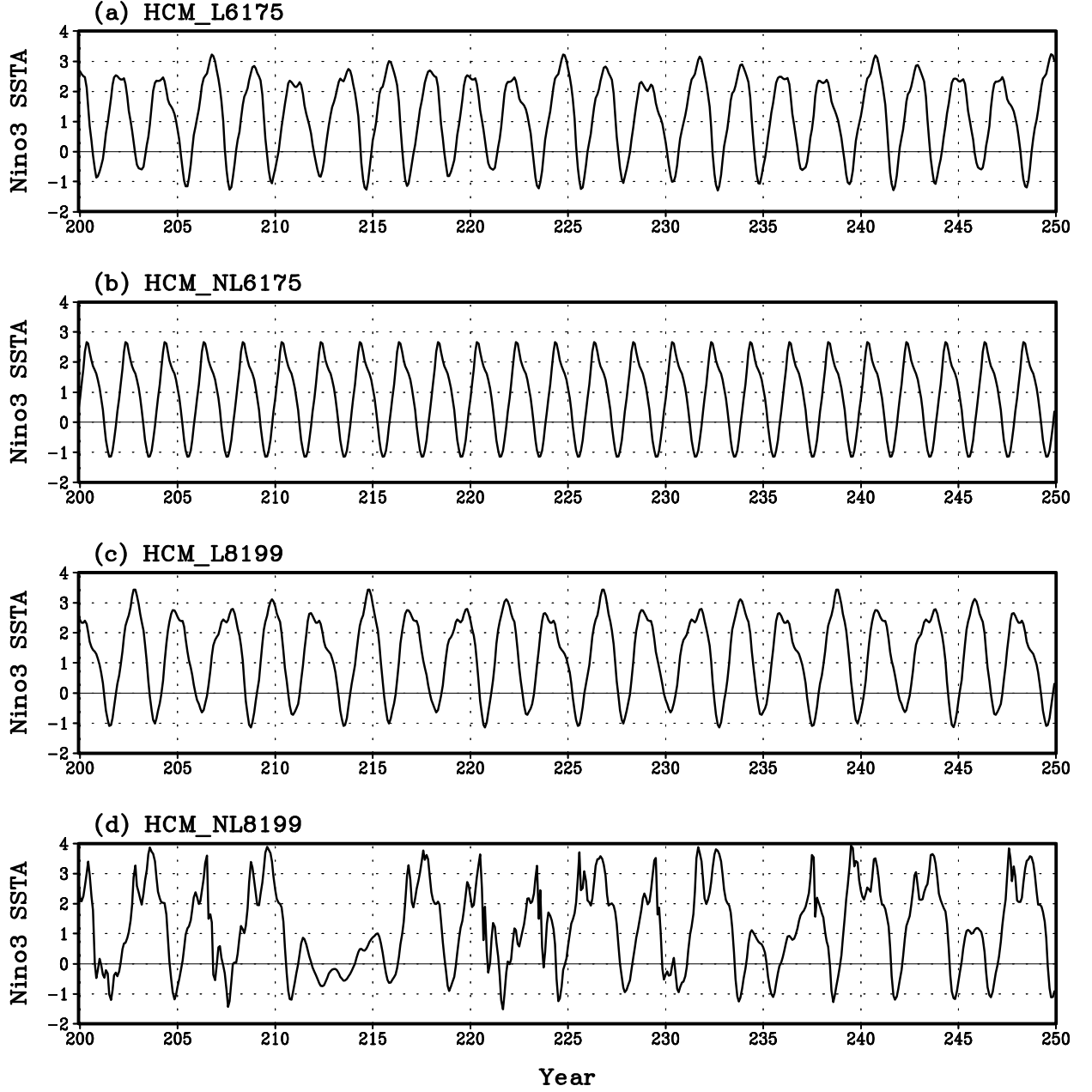Figure 5: Similar to Fig. 4 but for the CCA mode 1.

Figure 6: Time series of the Niño3 SST anomalies (in °C) simulated by 4 hybrid coupled models – HCM_{L6175}, HCM_{NL6175}, HCM_{L8199} and HCM_{NL8199}, as shown in panels a, b, c and d, respectively. All four models have the same Lamont ocean model, but the statistical atmosphere in (a) HCM_{L6175} is a CCA model built using data from 1961-75, and in (c) HCM_{L8199}, from 1981-99. The corresponding models using NLCCA are (b) HCM_{NL6175} and (d) HCM_{NL8199}.
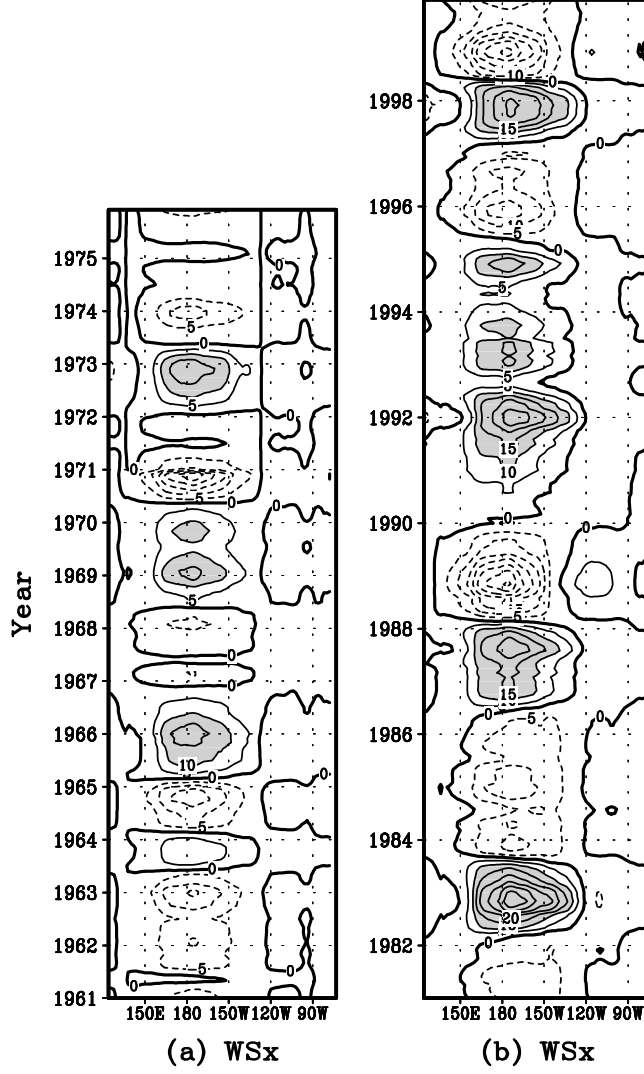
Figure 7: Time evolution of the equatorial zonal WS anomalies (averaged between 5°S and 5°N) predicted by the NLCCA models (only mode 1) using SST as predictor. Solid curves denote positive contours, dashed curves, negative contours, and thick curves, zero contours. The contour interval is $5\,m^2/s^2$. Areas with values greater than 10 are shaded. Panels (a) and (b) represent the 1961-75 and 1981-99 period, respectively.
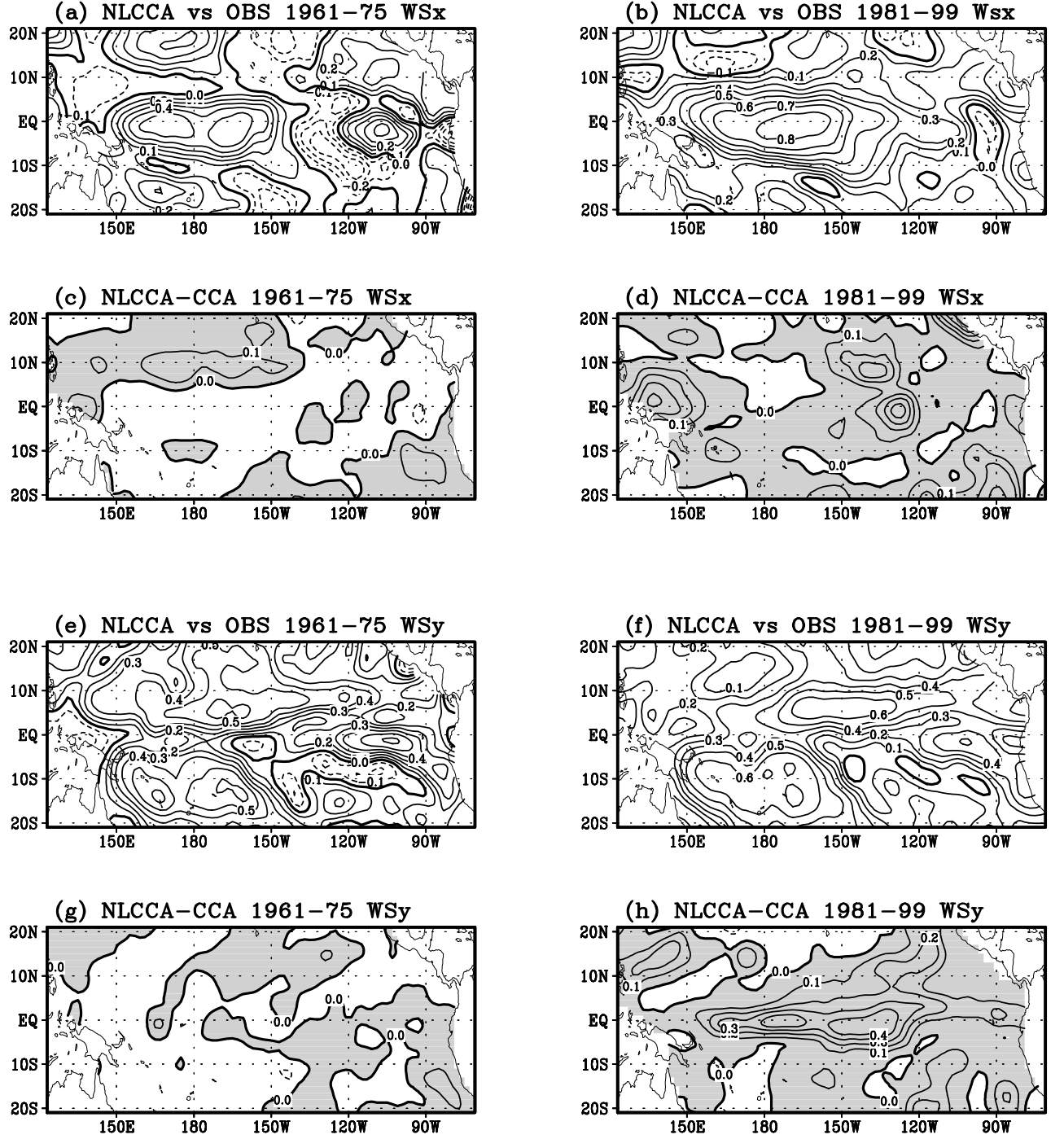
Figure 8: Distributions of the correlation skill of the WS anomalies predicted by the NLCCA models relative to the observations (Panels a, b, e and f) and the difference between the skill of NLCCA models and that of the corresponding CCA models (NLCCA minus CCA, panels c, d, g, and h). The 4 panels in the left column represent the period 1961-75, and the right column, the period 1981-99. The upper 4 panels represent the zonal component, and the lower 4 panels, the meridional component. The contour interval is 0.1 with positive skill difference shaded.
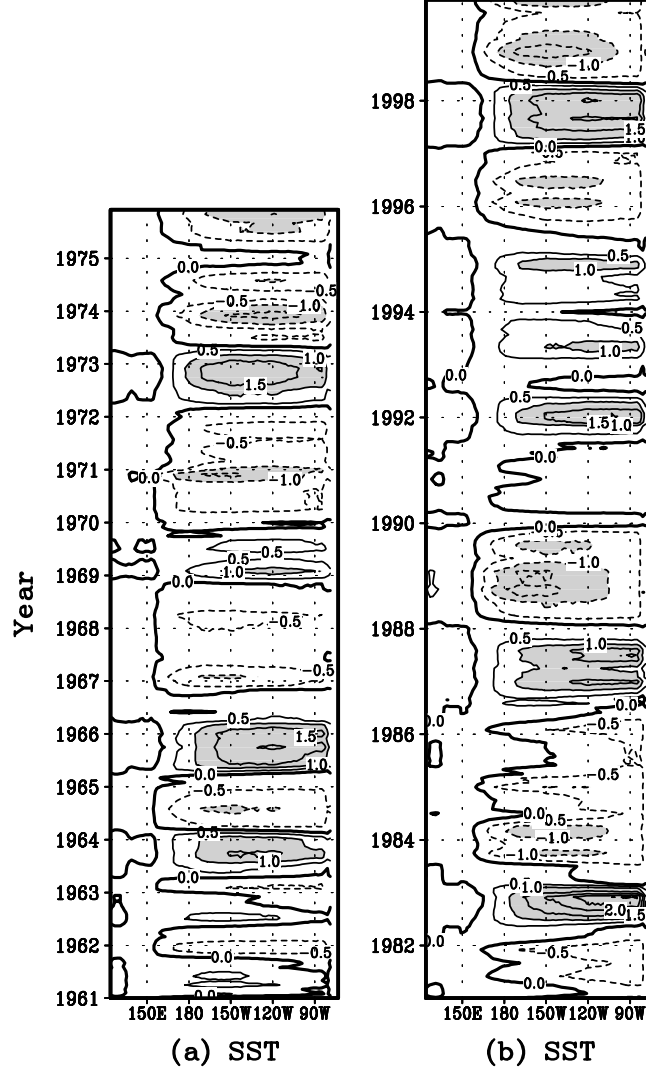
Figure 9: Time evolution of the equatorial SST anomalies (averaged between 5°S and 5°N) predicted by the NLCCA models (only mode 1) using WS as predictor. Solid curves denote positive contours, dashed curves, negative contours, and thick curves, zero contours. The contour interval is 0.5°C with values greater than +1.0°C shaded. Panels (a) and (b) represent the 1961-75 and 1981-99 period, respectively.